Open access • Journal Article • DOI:10.1109/TIE.2019.2913824

Design, Analysis, and Impacts of Sinusoidal LC Filter on Pulsewidth Modulated Inverter Fed-Induction Motor Drive — Source link

Prasun Mishra, Ramkrishan Maheshwari

Institutions: Indian Institute of Technology Delhi

Published on: 01 Apr 2020 - IEEE Transactions on Industrial Electronics (Institute of Electrical and Electronics Engineers)

Topics: Active filter, Filter (video), Filter capacitor, Ripple and Induction motor

Design, analysis, and impacts of sinusoidal LC filter on pulsewidth modulated inverter fed-induction motor drive

Mishra, Prasun; Maheshwari, Ramkrishan

Published in:
IEEE Transactions on Industrial Electronics

DOI:
10.1109/TIE.2019.2913824

Publication date:
2020

Document version:
Accepted manuscript

Citation for pulished version (APA):
Mishra, P., & Maheshwari, R. (2020). Design, analysis, and impacts of sinusoidal LC filter on pulsewidth modulated inverter fed-induction motor drive. *IEEE Transactions on Industrial Electronics*, *67*(4), 2678-2688. https://doi.org/10.1109/TIE.2019.2913824

Design, Analysis, and Impacts of Sinusoidal LC Filter on Pulse Width Modulated Inverter Fed Induction Motor Drive

Prasun Mishra, *Member, IEEE* and Ramkrishan Maheshwari, *Senior Member, IEEE*

***Abstract*— Squirrel cage induction motor (SQIM) fed by a pulse width modulated voltage source inverter (VSI) is subjected to voltage and current surges. It may cause additional losses in the motor, insulation failure, high bearing current, and electromagnetic interference. To mitigate these problems, sinusoidal LC filter is placed at the ac-side of the VSI. This paper proposes a new methodology to design the filter. In this method, the filter inductance is chosen based on the maximum ripple in the inverter ac-side current and the voltage drop across the filter inductor, and the filter capacitor is chosen based on the steady-state reactive power demand of the SQIM. The effects of the designed filter on the switch current, losses in the drive, temperature of the dc-link capacitor, dv/dt at the motor terminal, stator flux, and air-gap torque of the SQIM are discussed. The performance of the drive with the filters, designed by the proposed method and the standard method, are experimentally tested on a two-level Silicon carbide (SiC) VSI fed SQIM and comparative analysis is carried out. The impact of the designed filter on the drive is also shown when the neutral point of the filter capacitors is connected with the mid-point of the dc-link. The stability of the closed-loop controlled SQIM drive with the proposed filter, and simulation results are presented to verify its performance.**

Index Terms— Sinusoidal LC filter, squirrel-cage induction motor drive, variable-frequency operation.

I. Introduction

Silicon carbide (SiC) power metal–oxide–semiconductor field–effect transistor (MOSFET) based pulse width modulated voltage source inverter (VSI) has seen better technological prospects as compared to silicon (Si) power MOSFET based VSI [1]−[4]. These are also used in constant speed drives (CSD) and adjustable speed drives (ASD) [5]−[7]. As SiC MOSFET has the potential of fast switching transitions, it may aggravate the problems like insulation failure, high bearing current, severe electromagnetic interference (EMI), and a substantial amount of core losses in the VSI fed squirrel-cage induction motor (SQIM) drive [8]−[12].

To mitigate these problems, several filter configurations are proposed in the literature [13], [14]. Among those, the most popular configuration is three-phase second-order low-pass sinusoidal LC filter [15]−[16]. There are many methodologies available in the literature [17]−[21] to design the series filter inductor and the shunt filter capacitor. In [17], a three-phase LC filter with a band-reject circuit is optimally designed to minimize the cost of the filter with constraints like suppression of the switching harmonics and deviation of the fundamental output voltage. However, importance is given on the design of the filter inductor, while the effects of filter capacitance on ASD are ignored. An improved Genetic Algorithm optimization technique is used in [18] to select the filter inductance and the filter capacitance. In this method, the objective function is to minimize the harmonic distortion of the phase currents and phase voltages, the voltage drop across the inductor, the losses in the filter elements, and the cost of the filter. However, the effects of filter on power losses, cost, and size of the VSI are neglected. Similarly, an optimum design of the RLC filter using fuzzy logic is proposed in [19]. In this method, the switching time lag of the inverter and its operation in the overmodulation region are additionally considered in the design of the filter. The current through the filter capacitor is restricted to 10% of the rated current of the motor at its fundamental frequency to design the filter capacitor. However, the effect of the filter capacitor on the VSI is not discussed which significantly affects the performance of the drive. Another approach of designing sinusoidal LC filter for SiC VSI fed ac motor drive is used in [21], where the filter inductance is calculated by considering the voltage drop across the filter inductor at a certain percentage of the maximum operating fundamental frequency and the rated motor current. However, the design methodologies of [17]−[21] treat the filter elements separately and do not include the motor as a part of the system. Moreover, these procedures do not consider the effects of filter capacitance on the drive. As the filter capacitor may be used to supply the reactive power demand of the SQIM [15], it may reduce the inverter ac-side current. This may, in turn, reduce the power losses in the drive. Therefore, the effects of the filter capacitor on the drive have been considered in this paper.

In this paper, the filter capacitance has been calculated based on the reactive power demand of the SQIM at steady-state. The filter inductance is selected by considering two aspects like the ripple content in the inverter ac-side current and the voltage drop across the filter inductor. A preliminary discussion of the proposed method was presented in [23], where no experimental results were presented, and the impacts of the filter on different parts of the drive were not explored. The work of [23] has been extended in this paper, and the performance of the drive with the filters designed by the standard method (SM) and the proposed method (PM) has been verified at different operating points for an in-house designed and developed SiC MOSFET based three-phase VSI fed SQIM.

The following impacts of the filters designed by PM and SM are discussed, and comparative analysis is carried out:

1) The switch current of the VSI and the cumulative power loss in the drive with two filters have been discussed.
2) The effects of the two filters on the dc-link capacitor of the VSI have been discussed.

Manuscript received December 09, 2018 and revised March 14, 2019; accepted April 07, 2019.

The authors are with the department of Electrical Engineering, Indian Institute of Technology Delhi, New Delhi, India (e-mail: prasun210@gmail.com, rkmahesh@ee.iitd.ac.in.

3) The stator flux of SQIM, *dv/dt* at the motor-input terminals, and the pulsating electromagnetic air-gap torque of the SQIM with two filters have been discussed.
4) The common-mode voltages of the SQIM drive with two filters have been discussed when the neutral point of the filter capacitor is connected with the mid-point of dc-link.

This paper is organized as follows. The methodologies of designing LC filters by SM and PM are elaborated in Section II. The impacts of two filters, designed by SM and PM, on the VSI fed SQIM drive are theoretically analyzed in Section III and verified through experimental results in Section IV. The stability of the closed-loop motor drive with the filter at an operating point is briefly discussed and MATLAB simulation results are presented to verify its steady-state and dynamic performance in Section V followed by conclusion in Section VI.

II. Methods of LC Filter Design For VSI fed SQIM

In this paper, three-phase second-order low-pass sinusoidal LC filter has been designed for a SiC discrete MOSFET based three-phase two-level VSI fed 3 hp, 415 V, 4.6 A, four-pole, 50 Hz, star connected, three-phase SQIM as shown in Fig. 1. Here, R_f and L_f are the per-phase ac resistance and inductance of the filter inductor, respectively. R_c, and C_f are the per-phase ac resistance and capacitance of the filter capacitor, respectively. The calculation of the filter inductance is common in both SM and PM. However, the calculation of the filter capacitance is different in SM and PM, which is discussed in the following sub-sections.

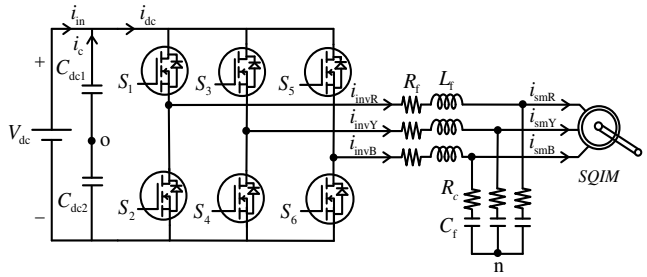

Fig. 1. VSI fed three-phase SQIM with sinusoidal LC filter.

A. Calculation of Filter Inductance (L_f) in SM and PM

The magnitude of L_f has been calculated considering two design criteria [20]−[22]. The first criterion [20] is that the value of switching ripple current (Δi_{inv}) through L_f is within 15−25 % of the peak value of the inverter ac-side current (i_{inv}). i_{inv} is assumed as the rated current (i_{sm}) of SQIM. The second criterion [21], [22] is that the voltage drop (v_L) across L_f at rated i_{inv} and rated frequency (f_s) should not exceed 3% of the rated motor voltage (v_{sm}). However, the selection of L_f is basically a design trade-off between the maximum current ripple and the size of L_f. The expressions of Δi_{inv} and v_L are given by

$$\Delta i_{inv} = \frac{V_{dc}}{8 \times f_{sw} \times L_f} \tag{1}$$

$$v_L = i_{inv}\left(\sqrt{{R_f}^2 + \left(2\pi f_s L_f\right)^2}\right) \tag{2}$$

where V_{dc} is the dc-link voltage and f_{sw} is the switching frequency. The value of Δi_{inv} is considered as 20% of the peak value of rated i_{inv}. The calculated value of L_f is 1.15 mH for V_{dc} = 600 V and f_{sw} = 50 kHz. However, L_f of 1.2 mH has been used in experiment which is closer to the calculated value. v_L across L_f (L_f =1.2 mH, R_f = 0.3 Ω) is 0.93 % at v_{sm} =239.60 V, i_{inv} = 4.6 A, and f_s = 50 Hz.

B. Calculation of Filter Capacitance (C_f) in SM

Fig. 2 depicts the power circuit [22] which has been considered to calculate the filter parameters in SM where L_f, C_f, stator and rotor leakage inductance (L_{ls} =14.1 mH and L_{lr} =14.1 mH) of SQIM are only considered to find out the Thevenin equivalent inductance (L_{eq}) as these inductances play major role at higher frequency than the magnetizing inductance (L_m= 267 mH) of the SQIM. v_{inv} is the inverter output voltage.

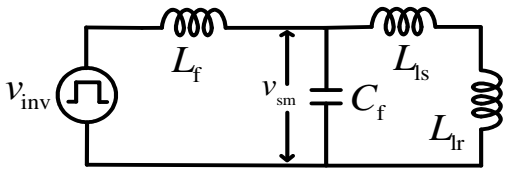

Fig. 2. Power circuit considered in SM to calculate filter parameters.

The expression of effective resonance frequency (f_{res}) is given by

$$f_{res} = \frac{1}{2\pi\sqrt{L_{eq}C_f}} = \frac{1}{2\pi}\cdot\sqrt{\left(\frac{L_f + L_l}{L_f L_l C_f}\right)} \tag{3}$$

where, L_l is the summation of L_{ls} and L_{lr}. Once the value of L_{eq} is calculated, the value of C_f can also be calculated by (3) for a chosen f_{res}. In order to avoid the resonance frequency oscillation, it is advisable to choose f_{res} below the switching frequency and well above the fundamental frequency of the pulse width modulated inverter output voltage [24]. For f_{sw} of 50 kHz and f_s of 50 Hz, f_{res} is chosen as 5 kHz to reduce the size of C_f. The value of C_f is calculated as 0.845 µF. However, C_f of 1.25 µF is used in the experiment which is closer to the calculated value and f_{res} is recalculated as 4195.90 Hz. In SM, the filter is only responsible for filtering high-frequency components and the effects of C_f on the ac drive are not explored. However, the value of C_f in PM has been calculated by considering its impacts on the ac drive as discussed below.

C. Calculation of Filter Capacitance in PM

The basic motivation behind PM is that the reactive power demand of the SQIM has to be supplied by C_f and only the active power demand has to be supplied from the VSI. The reactive power is mainly responsible for energizing the magnetic core of the SQIM to develop the required air-gap flux and its demand is almost same irrespective of no-load or full-load operation. As the reactive power demand is higher as compared to the active power demand of the SQIM at 50 Hz and no-load operation, the no-load power factor (p.f) of the SQIM is poor as compared to its full-load p.f. The reactive power demand at 50 Hz is almost fixed irrespective of load. Therefore, reactive elements of per-phase steady-state no-load equivalent circuit of the motor and filter are only considered in PM for equalizing the reactive power demand of SQIM and the reactive power supplied by C_f. Fig. 3 depicts the power circuit which has been considered to calculate the filter parameters in PM where L_f, L_{ls}, and L_m have been considered. v_{sm} is the stator phase voltage of the SQIM.

In PM, the active power demand of the SQIM and the reactive power demand of L_f are supplied from the VSI, while the reactive power demand of the SQIM is supplied from the filter capacitor, i.e.,

$$v_{sm}^{\ 2} \times 2\pi f_s C_f = \frac{v_{sm}^{\ 2}}{2\pi f_s \left(L_m + L_{ls}\right)} \tag{4}$$

The value of C_f is deduced from (4) and is given by

$$C_f = \frac{1}{4\pi^2 f_s^{\ 2}\left(L_m + L_{ls}\right)} \tag{5}$$

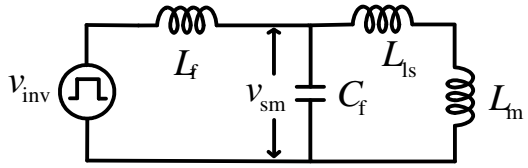

Fig. 3. Power circuit considered in PM to calculate filter parameters.

The value of C_f is calculated as 35.99 µF when f_s and L_m are 50 Hz and 267 mH, respectively. However, C_f of 40 µF is used in the experiment which is closer to the calculated value. The f_{res} in PM is calculated as 741.73 Hz for the chosen filter inductance and filter capacitance. The calculated values of L_f, C_f, and f_{res} in PM and SM have been tabulated in Table I.

TABLE I
PARAMETERS OF FILTER OBTAINED BY SM AND PM

Method	f_s (Hz)	f_{sw} (kHz)	f_{res} (Hz)	L_f (mH)	C_f (µF)
SM	50	50	4195.90	1.2	1.25
PM	50	50	741.73	1.2	40

The 40 µF filter capacitor (EUROPTRONIC MPX2) in PM is 32 times higher than the 1.25 µF filter capacitor (CTR MPPRRB) in SM. 40 µF capacitor in PM is realized by connecting four 10 µF capacitors in parallel. However, parallel connection of capacitors reduces effective equivalent series resistance (ESR) of the capacitor bank and also increases its current rating. The volume and unit price of 1.25 µF capacitor are 13.125 cm^3 and 0.24 USD, respectively. The volume and unit price of 40 µF capacitor bank are 216 cm^3 and 2.52 USD, respectively. The 40 µF capacitor bank can also be replaced by a single 40 µF capacitor. The volume and unit price (minimum order of 100 units) are different if these capacitors are manufactured by VISAY and EPCOS. The volume and unit price of a 2 µF ac film filter capacitor (MKP1847520254K2) are 7.39 cm^3 and 2.75 USD, respectively. The volume and unit price of a 40 µF ac film filter capacitor (B32796E2406K) are 56.70 cm^3 and 16.11 USD, respectively. However, the larger volume and higher cost of the filter capacitor in PM than SM are compensated by following long-run favorable outcomes as discussed below.

III. IMPACTS OF FILTER (THEORETICAL ANALYSIS)

The LC filter designed by PM has significant impacts on the VSI fed SQIM drive in comparison with the filter designed by SM. These impacts are discussed in the following sub-sections with MATLAB simulation results. The fundamental frequency (f_s : 10−50 Hz) of the motor line-line voltage ($v_{sm(L)}$: 83−415V) and the load torque (m_l : 0−10 Nm) of the SQIM drive with filter have been varied in open loop *v/f* control.

A. Reduction of ac-side current (i_{inv}) of VSI

In PM and SM, the magnitude of i_{inv} at different frequencies and load torques have been plotted in Fig. 4. The magnitude of i_{inv} is significantly reduced in PM than that of SM from medium-frequency to the high-frequency operation of the SQIM. In low-frequency, the filter capacitor does not fully compensate the reactive power demand of *v/f* controlled SQIM as the frequency and the voltage of the filter capacitor are reduced proportionally. However, the magnitude of i_{inv} at all operating frequencies is always lesser in PM than SM. For example, it is in the range of 1.45 A to 3.59 A in PM and 2.89 A to 4.53 A in SM while m_l is varied from 0 Nm to 10 Nm at 50 Hz.

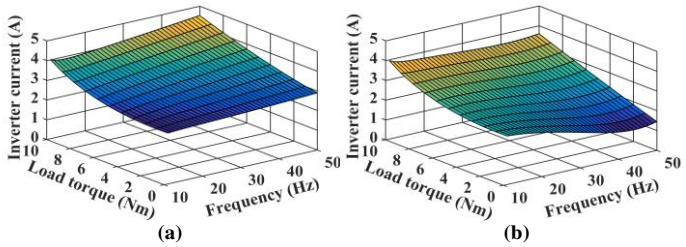

Fig. 4. Magnitude of i_{inv} at variable m_l and f_s in (a) SM, (b) PM.

For a balanced ac-side phase current of the VSI, the root mean square (rms) current through MOSFET ($I_{rms,M}$) and anti-parallel diode ($I_{rms,D}$) [25] are given by

$$I_{rms,M} = \frac{I_{rms}}{2}\sqrt{\left(1 + \frac{8m_a\cos(\phi)}{3\pi}\right)} \tag{6}$$

$$I_{rms,D} = \frac{I_{rms}}{2}\sqrt{\left(1 - \frac{8m_a\cos(\phi)}{3\pi}\right)} \tag{7}$$

where, I_{rms} is the rms value of i_{inv}, m_a is the modulation index, and $\cos(\phi)$ is the p.f. As the value of I_{rms} for same m_a is lesser in PM than that of SM as shown in Fig. 4, the current through the switch (MOSFET and antiparallel diode) is lesser in PM than SM. The reduced ac-side current (i_{inv}) of the VSI in PM than that of SM also reduces the cumulative loss in the VSI and filter and thus it improves the efficiency of the whole drive. Experimental results are presented in Section IV.

B. Reduction of rms current ripple and temperature rise of dc-link capacitor

For same m_a, I_{rms} of i_{inv} is reduced and $\cos(\phi)$ is increased in PM than SM. The expression of rms value of the dc-link capacitor-current ripple ($i_{c,rms}$) is given by [26]

$$i_{c,rms} = I_{rms}\sqrt{2m_a\left[\frac{\sqrt{3}}{4\pi} + \cos^2(\phi)\left(\frac{\sqrt{3}}{\pi} - \frac{9}{16}m_a\right)\right]} \tag{8}$$

Therefore, the variation of $i_{c,rms}$ in PM and SM are calculated by (8) and are shown in Fig. 5. The magnitude of $i_{c,rms}$ is significantly reduced in medium-frequency and high-frequency region as compared to the low-frequency region. However, its magnitude at all fundamental frequencies is lesser in PM than that of SM. For example, it is in the range of 0.73 A to 1.81 A in PM and 1.50 A to 2.31 A in SM while m_l is varied from 0 Nm to 10 Nm at 50 Hz.

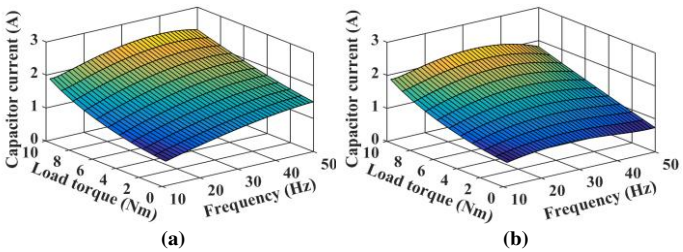

Fig. 5. $i_{c,rms}$ at variable m_l and f_s in (a) SM, (b) PM.

Six BLC polypropylene board mount 16 µF film capacitor (Part No: BLC160J901B4C) connected in series-parallel combination have been used as dc-link capacitors. Two capacitors (C_d) are connected in series and three such configurations are connected in parallel to form total dc-link capacitance (C_{dc}) where C_{dc}=1.5C_d. The parameters of the capacitors are given in [27]. The rms ripple current (i_{crms}) through an individual capacitor (C_d) is the 1/3rd time of the current flows through the equivalent capacitor (C_{dc}) and the temperature difference (ΔT) between the ambient (T_a) and the core (T_c) of each capacitor (C_d) is calculated by

$$\Delta T = T_c - T_a = \sum \left(i_{crms,f}^2 \times ESR_f \times \theta_f \right) \tag{9}$$

where θ_f is the total thermal resistance, ESR_f is the ESR of the capacitor, and $i_{crms,f}$ is the ripple current through the capacitor at the frequency (f). Expected lifetime of the capacitor for same operating voltage mainly depends on the core temperature of the dc-link capacitor as given by [28]

$$L_p = L_r \times \left(\frac{V_a}{V_r} \right)^{-n} \times 2^{\frac{(T_r - T_c)}{10}} \tag{10}$$

where, L_p and L_r are the predicted and the rated lifetime of the capacitor, respectively. T_c and T_r are the temperature in Kelvin at the operating condition and rated condition, respectively. V_a and V_r are the voltages at the operating condition and rated condition, respectively. According to (9) and (10), lesser high-frequency $i_{c,rms}$ in PM than SM also reduces the temperature rise and experimental results at the same operating point are presented in Section IV for comparison.

C. Reduction of distortions in stator-flux of SQIM

The filter, having lower f_{res} in PM than SM, highly attenuates the harmonic components of v_{inv} and produces less distorted v_{sm} and i_{sm}. Therefore, the less distorted alpha (α) and beta (β) component of v_{sm} ($v_{sα}$, $v_{sβ}$) and i_{sm} ($i_{sα}$, $i_{sβ}$) produce less distorted alpha (α) and beta (β) component of stator flux ($\lambda_{sα}$, $\lambda_{sβ}$) [29] as given by

$$\lambda_{sx} = \int \left(v_{sx} - R_s i_{sx} \right) dt \ , \ x = \{\alpha, \beta\} \tag{11}$$

where R_s is the per phase stator resistance of the SQIM. In Section IV, it is experimentally verified and compared at the same operating point in an open-loop *v/f* controlled SQIM drive with filters designed by SM and PM.

D. Reduction of air-gap torque pulsation of SQIM

The harmonic voltages produce harmonic currents as well as harmonic fluxes. The interactions between fundamental and harmonic components of fluxes and currents produce pulsating air-gap torque in SQIM. It deteriorates the performance of the SQIM and creates mechanical vibration and noise. In [30], the expression of pulsating air-gap torque of SQIM drive is derived by considering all kind of harmonics which may be present in the balanced system. The filtered inverter voltage has j^{th} order positive, k^{th} order negative and p^{th} order zero sequence harmonic components with respect to its fundamental component depending on the dead time of the VSI, cutoff frequency, and gain of the filter. Here, j = 6q+1, k = 6q-1, and p = 3q for q = 0, 1, 2, 3 and so on. The dc component of the air-gap torque [30] is given by

$$T_e = T_{dc} = \frac{2}{3} \frac{P}{2} \frac{v_{sm1} i_{sm1}}{\omega} \cos(\phi_1) \tag{12}$$

where ϕ_1 is the phase angle between the fundamental component of motor phase voltage (v_{sm1}) and motor phase current (i_{sm1}). The air-gap torque equation with negative sequence harmonics [30] is given by

$$t_e(t) = T_{dc} + T_{j+1Neg} \cos((j+1)\omega t + \phi_j) \tag{13}$$

where $T_{j+1Neg} = \frac{2}{3} \frac{P}{2} \left(\frac{v_{sm1} i_{smj}}{\omega} - \frac{v_{smj} i_{sm1}}{j\omega} \right)$

The air-gap torque equation with positive sequence harmonics [30] is given by

$$t_e(t) = T_{dc} + T_{k-1Pos} \cos((k-1)\omega t + \phi_k) \tag{14}$$

where $T_{k-1Pos} = \frac{2}{3} \frac{P}{2} \left(\frac{v_{sm1} i_{smk}}{\omega} + \frac{v_{smk} i_{sm1}}{k\omega} \right)$

At very high frequency, the contribution of the terms having j and k in the denominator of negative (T_{j+1Neg}) and positive sequence (T_{k-1Pos}) torque components in (13) and (14), respectively are negligible in the air-gap torque equation. Therefore, the air-gap torque is considered as the product of the stator-current and fundamental component of stator-flux. As the fundamental current and the fundamental voltage profile of the SQIM are improved in the PM than SM due to higher filter capacitance, the air-gap torque profile is improved in PM. In Section IV, it is experimentally verified and compared at the same operating point in an open-loop v/f controlled SQIM drive with the filters designed by SM and PM.

E. Reduction of common mode voltage (special case)

If the neutral point (n) of the filter capacitors is connected with the mid-point (o) of the dc-link, the expression of common-mode voltage (v_{cm}) is derived in [31] and is given by

$$v_{cm} = \frac{v_{sRg} + v_{sYg} + v_{sBg}}{3} = \frac{1}{3} \left(R_c i_o + \frac{1}{C_f} \int i_o dt \right) + v_{og} \tag{15}$$

where v_{og} is the voltage between the supply ground (g) and mid-point (o) of dc-link. i_o is the total current flowing from "n" to "o". v_{sRg}, v_{sYg}, and v_{sBg} are the stator voltages of phase R, Y, and B w.r.t ground, respectively. It is clear from (15) that the magnitude of v_{cm} depends on the filter parameters (R_c, C_f) and i_o, and it is experimentally verified and compared in Section IV.

F. Reduction of dv/dt at motor terminal

The time derivative of stator voltage is inversely proportional to the square root of filter capacitance of the LC filter [32] and is given by

$$\frac{dv_{sm}}{dt} = \frac{V_{dc}}{\sqrt{L_{eq}C_f}} \quad (16)$$

Higher filter capacitance in PM than that of SM is also beneficial from the *dv/dt* aspect, as it reduces the rate of rise of the motor terminal voltage and it is experimentally verified and compared in Section IV.

IV. Impacts of Filter (Experimental Results)

All the experiments have been performed on SiC MOSFET based VSI fed SQIM without and with LC filter designed by PM and SM, as shown in Fig. 6. The iron powder toroidal core and ac polypropylene film capacitors have been used to design the LC filters. The open loop *v/f* control of the SQIM with space vector pulse width modulation (SVPWM) technique has been implemented in TMS320F28335 digital signal controller (DSC).

Fig. 6. (a) SiC MOSFET based VSI, (b) filter inductors and capacitors and, (c) TMS320F28335 DSC and signal conditioning circuits.

The values of f_{sw} and V_{dc} are 50 kHz and 600 V, respectively. The values of m_a and dead-time of the VSI are set to 1 and 1 µs, respectively. The frequency reference of the *v/f* controlled drive with and without filter is set to 50 Hz. The performance of the drive with LC filters designed by SM and PM have been compared and analyzed in the following sub-sections.

A. Reduction of ac-side current (i_{inv}) of VSI

Figs. 7–9 and Figs. 10–12 show the line current (i_{sm} and i_{inv}) and the line-line voltage ($v_{sm(L)}$ and $v_{inv(L)}$) of the motor and inverter at 50 Hz with light and full load torque. The experimental results as shown in Figs. 7–12 have been analyzed by Fast Fourier Transform (FFT) and the rms value of the fundamental currents and voltages as well as the percentage (%) total harmonic distortion (THD) have been tabulated in Table II–III. The oscillations in i_{inv} of Fig. 12 near about f_{res} (741.73 Hz) is due to the resonance of LCL network. The magnitude of the fundamental $v_{inv(L)}$ is reduced due to dead-time effect [33]. The magnitude of i_{inv} with light load operation is 1.737 A without filter, 1.612 A, and 0.7298 A with the filters, designed by SM and PM, respectively. The magnitude of i_{inv} with full load operation is 5.063 A without filter, 4.756A, and 4.163 A with filters, designed by SM and PM, respectively.

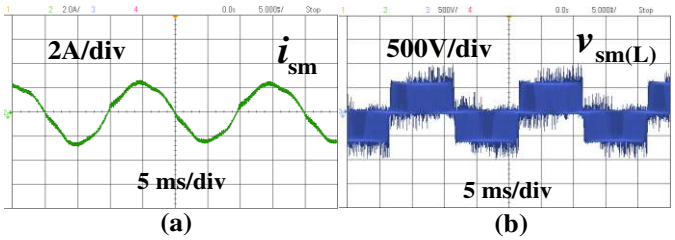

Fig. 7. Experimental results at 50 Hz without filter and light load, (a) i_{sm} (2A/div), (b) $v_{sm(L)}$ (500V/div).

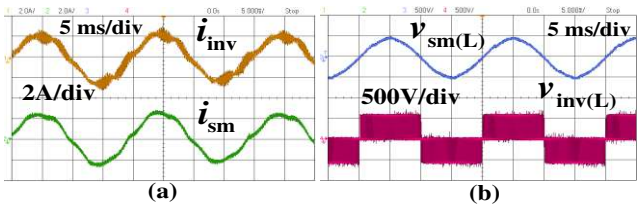

Fig. 8. Experimental results at 50 Hz with filter and light load in SM, (a) i_{sm}, i_{inv} (2A/div), (b) $v_{sm(L)}$, $v_{inv(L)}$ (500V/div).

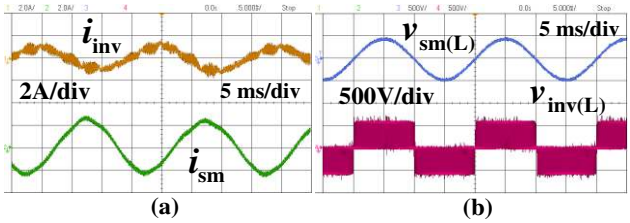

Fig. 9. Experimental results at 50 Hz with filter and light load in PM, (a) i_{sm}, i_{inv} (2A/div), (b) $v_{sm(L)}$, $v_{inv(L)}$ (500V/div).

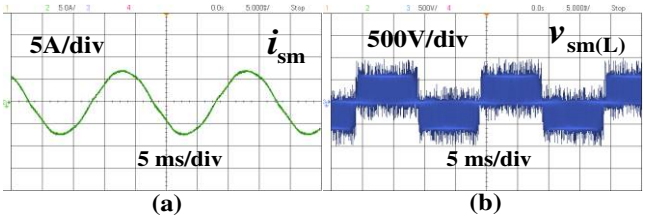

Fig. 10. Experimental results at 50 Hz without filter and full load, (a) i_{sm} (5A/div), (b) $v_{sm(L)}$ (500V/div)

TABLE II
Comparison With Light Load Torque at 50 Hz

Method	i_{inv} (A)	i_{sm} (A)	$v_{inv(L)}$ (V)	$v_{sm(L)}$ (V)
No filter	1.737	1.737	338.3	338.3
	(9.18%)	(9.18%)	(75.27%)	(75.27%)
SM	1.612	1.689	334.7	330.3
	(17.85%)	(10.62%)	(73.62%)	(4.51%)
PM	0.7298	1.64	324.8	322.7
	(37.76%)	(9.04%)	(75.26%)	(3.72%)

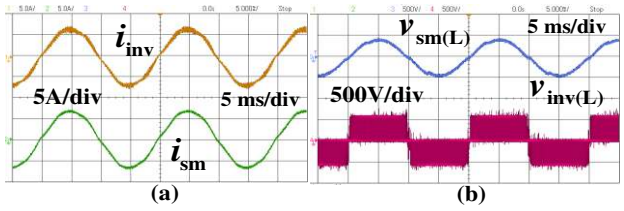

Fig. 11. Experimental results at 50 Hz with filter and full load in SM, (a) i_{sm}, i_{inv} (5A/div), (b) $v_{sm(L)}$, $v_{inv(L)}$ (500V/div).

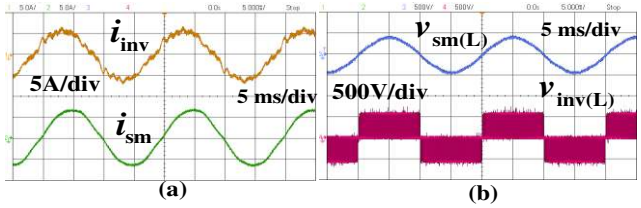

Fig. 12. Experimental results at 50 Hz with filter and full load in PM, (a) i_{sm}, i_{inv} (5A/div), (b) $v_{sm(L)}$, $v_{inv(L)}$ (500V/div).

The waveforms of i_{inv} and i_{sm} at 25 Hz with light and medium load torque operation are shown in Figs. 13–14. The magnitude of i_{inv} with light load operation is 1.484 A and 1.052 A with the filters designed by SM and PM, respectively. The magnitude of

i_{inv} with medium load operation is 3.720 A and 3.592 A with the filters designed by SM and PM, respectively. The distortion in the current waveforms, as shown in Figs. 7−14, is due to dead-time effect and it also varies with the modulation index and fundamental frequency [33]. The fundamental output voltage of the VSI is found less because of the voltage deviation in PM than SM as the power factor of the drive is improved in PM.

TABLE III
COMPARISON WITH FULL LOAD TORQUE AT 50 HZ

Method	i_{inv} (A)	i_{sm} (A)	$v_{inv\,(L)}$ (V)	$v_{sm\,(L)}$ (V)
No filter	5.063	5.063	305.7	305.7
	(3.27%)	(3.27%)	(83.24%)	(83.24%)
SM	4.756	4.784	305.8	299.9
	(7.98%)	(4.27%)	(81.87%)	(5.37%)
PM	4.163	4.718	301.5	296.7
	(9.23%)	(3.88%)	(84.43%)	(4.57%)

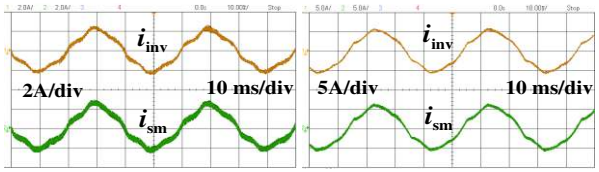

Fig. 13. Experimental results at 25 Hz with filter in SM, (a) i_{sm}, i_{inv} (2A/div) at light load, (b) i_{sm}, i_{inv} (5A/div) at medium load.

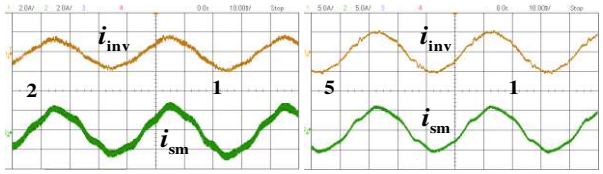

Fig. 14. Experimental results at 25 Hz with filter in PM, (a) i_{sm}, i_{inv} (2A/div) at light load, (b) i_{sm}, i_{inv} (5A/div) at medium load.

The cumulative power losses in the VSI and LC filter designed by SM and PM are measured from the experimental set up at 50 Hz with light and full load torque. The combined efficiency (η) is then calculated from the input power (P_{in}) and output power (P_o) of the VSI and filter as tabulated in Table IV.

TABLE IV
LOSS IN VSI AND FILTER AT 50 HZ, LIGHT AND FULL LOAD

Method	i_{sm} (A)	P_{in} (W)	P_o (W)	η (%)	p.f of SQIM
SM	1.689	337.67	270.54	80.12	0.28
	4.784	2251.03	2161.89	96.04	0.87
PM	1.64	310.60	256.65	82.63	0.28
	4.718	2160.08	2109.32	97.65	0.87

Therefore, the SQIM drive with proposed filter gives best performance for constant speed drives (CSD) like conveyor belts, compressors, spinning and ginning process of textile industry, mine hoist load, renewable energy-based water heating and cooling system, renewable energy based water pumping system, industrial exhaust blowers, locomotive radiator fans etc. For example, three-phase SQIM drive with the filter in water pumping is mostly operated at rated speed with variable load cycle. In such CSD applications, the SQIM drive with the proposed filter gives always better performance than the standard filter. The filter capacitance in PM can be calculated for designed operating frequency based on the customer's requirement. In ASD applications, the SQIM drives are operated at different operating speeds with variable load cycles. The operation continues throughout the year to meet the load demands. If the daily, weekly, monthly or yearly cumulative energy consumption is considered, then the SQIM drive with the proposed filter consumes lesser energy from the utility grid supply by reducing the cumulative losses in the drive as compared to the SQIM drive with the standard filter. Therefore, this solution increases the cumulative efficiency of the drive and this in turn will reduce the electricity bill in the long run.

B. Reduction of temperature of dc-link capacitor

The inverter-input-current (i_{dc}) is given by [26]. The i_{dc} in the experiment is estimated by (17) in DSC from sensed three-phase inverter currents (i_{inv}) and switching pulses (S_1, S_3, S_5) of the VSI.

$$i_{dc} = (S_1 \times i_{invR}) + (S_3 \times i_{invY}) + (S_5 \times i_{invB}) \quad (17)$$

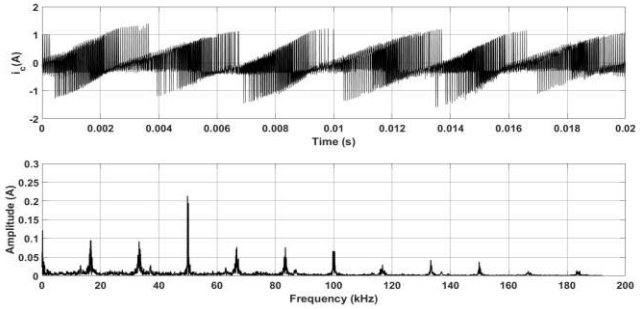

Fig. 15. i_c and it's FFT at 50 Hz without filter and light load.

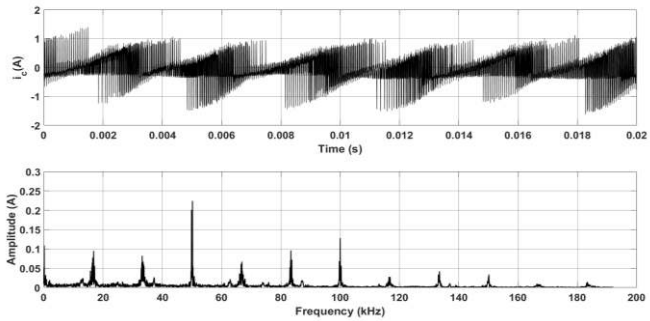

Fig. 16. i_c and it's FFT at 50 Hz with filter and light load in SM.

The ac ripple component of i_{dc} is the ripple current (i_c) through C_{dc}. The waveforms of i_c for three cases (without filter, SM, and PM) are shown in Figs. 15−20.

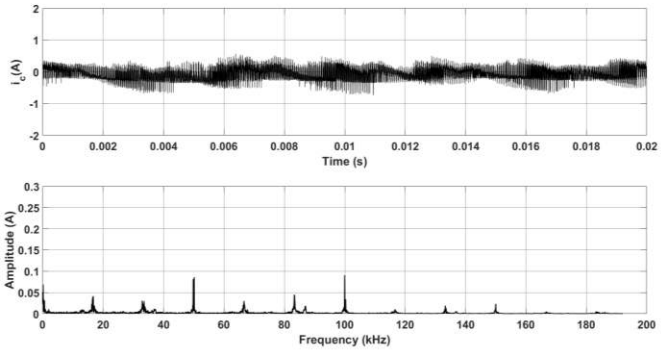

Fig. 17. i_c and it's FFT at 50 Hz with filter and light load in PM.

The different frequency components of i_c have been extracted by FFT analysis. The ESR as well as θ_f have also been calculated at different frequencies. The instantaneous temperature rise in each dc-link capacitor is calculated by (9) and tabulated in Table V. The magnitudes of different frequency components of i_c and the corresponding frequency dependent ESR are reduced in PM than SM with light load and with full load, respectively. Therefore, ΔT in C_d is less in PM than SM and it may lengthen the lifetime of the dc-link capacitor [27]−[28].

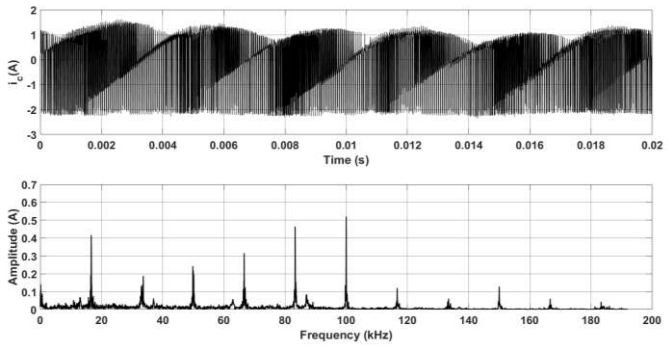

Fig. 18. i_c and it's FFT at 50 Hz without filter and full load.

TABLE V
CALCULATED ΔT IN INDIVIDUAL CAPACITOR (C_d)

Load torque	ΔT without filter	ΔT in SM	ΔT in PM
Light load	0.0026 °C	0.0026 °C	0.0006 °C
Full load	0.0154 °C	0.0162 °C	0.0127 °C

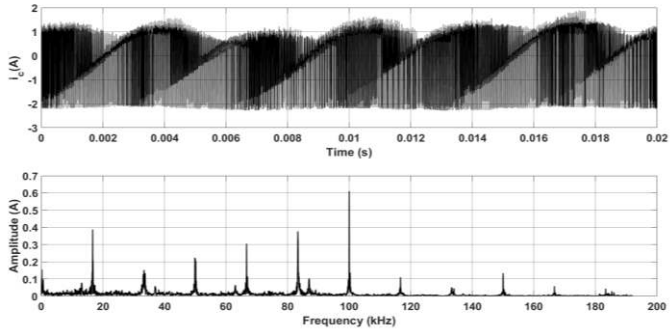

Fig. 19. i_c and it's FFT at 50 Hz with filter and full load in SM.

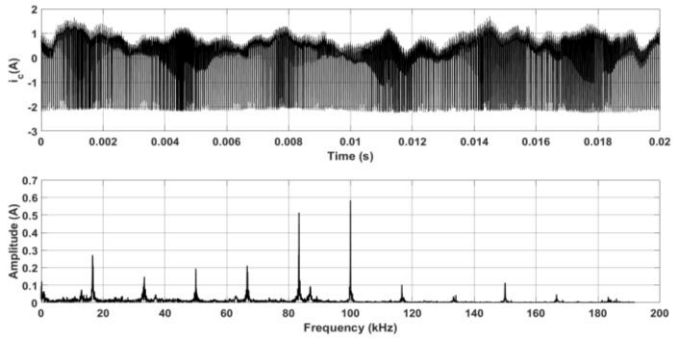

Fig. 20. i_c and it's FFT at 50 Hz with filter and full load in PM.

C. Reduction of distortion in stator-flux of SQIM

In the experimental setup, the stator-flux of SQIM has been estimated using (11) from the sensed stator-voltages and stator-currents. The alpha and beta components of the estimated stator-flux vector in SM and PM are plotted in Figs. 21−22 for light load and full load operation of SQIM. The distortion in the stator-flux trajectory has been reduced in PM than SM and therefore improves the stator-flux of the SQIM. It could be seen from Table II−III that the % THD of the stator-voltage and stator-current are also reduced.

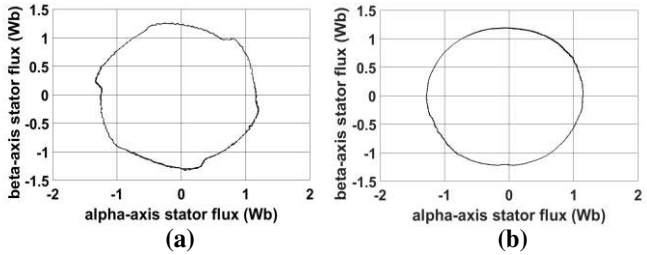

Fig. 21. Stator-flux trajectory of SQIM with light load in (a) SM, (b) PM.

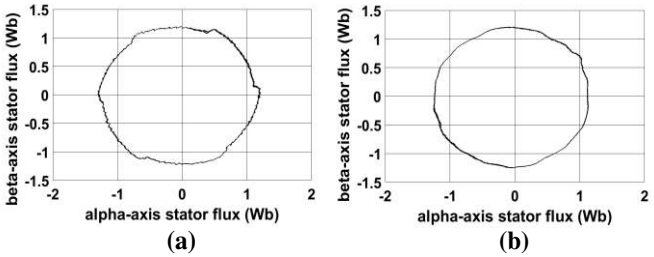

Fig. 22. Stator-flux trajectory of SQIM with full load in (a) SM, (b) PM.

D. Reduction of air-gap torque pulsation of SQIM

The air-gap torque of the SQIM [30] in the experiment is estimated offline from the stator currents and the fundamental stator flux, where the stator-voltages and stator-currents of SQIM are sensed from the experimental setup. The estimated air-gap torque and the zoomed version of its frequency spectrums are shown in Figs. 23−24.

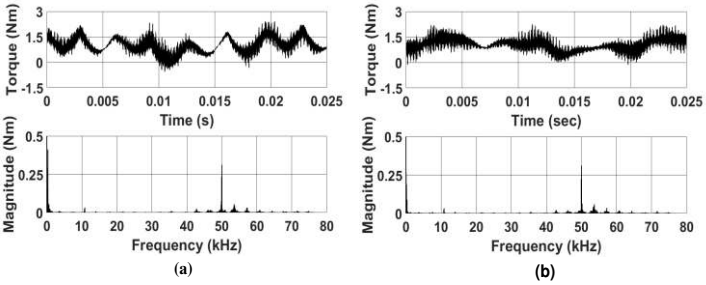

Fig. 23. Air-gap torque and its FFT with light load in, (a) SM, (b) PM.

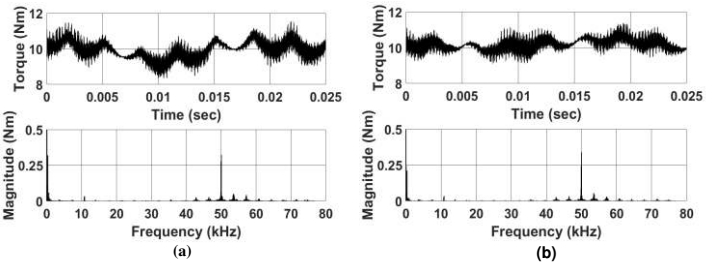

Fig. 24. Air-gap torque and its FFT with full load in, (a) SM, (b) PM.

The torque ripple over one cycle of f_s is calculated by subtracting the average of estimated torque from the actual estimated torque, and those are tabulated in Table VI-VII. It is found that the dominant frequency components of the air-gap torque have been comparatively reduced in PM than SM. Therefore, the torque pulsation has been comparatively reduced in PM than SM. The presence of low order frequency

components in voltage and current of the inverter, as well as the motor, is due to the dead-time of the inverter [33].

TABLE VI
COMPARISON OF DIFFERENT COMPONENTS IN TORQUE

Load	Light load		Full load	
Frequency	300 Hz	50050 Hz	300 Hz	50050 Hz
SM	0.4117 Nm	0.3117 Nm	0.3200 Nm	0.3250 Nm
PM	0.0896 Nm	0.3103 Nm	0.2111 Nm	0.3281 Nm

TABLE VII
COMPARISON OF AVERAGE TORQUE AND TORQUE RIPPLE

Load	Light load		Full load	
Torque	Average torque	Torque ripple	Average torque	Torque ripple
SM	0.9504 Nm	0.5138 Nm	9.9254 Nm	0.5576 Nm
PM	1.008 Nm	0.4038 Nm	10.178 Nm	0.4142 Nm

E. Reduction of common mode voltage (special case)

The effect of the higher value of filter capacitance on v_{cm} in PM than SM has been shown through experimental results. In the experiment, the three-phase stator voltages of the SQIM w.r.t supply ground have been sensed and the common mode voltage (v_{cm}) has been calculated by (15). The peak-peak v_{cm} is found 140 V and 164 V in PM and SM, respectively as shown in Fig. 25. However, the harmonics present in i_o in such filter configuration [31] increases the ripple content in i_{inv} as shown in Fig. 26 and thus increases the ripple content in i_c.

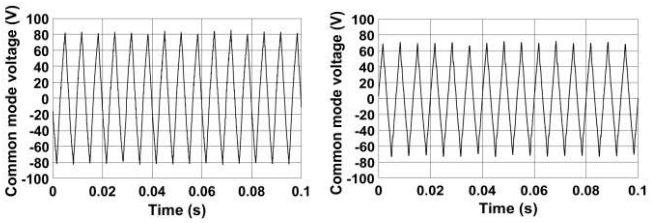

Fig. 25. Common mode voltage (v_{cm}) w.r.t ground in (a) SM, (b) PM.

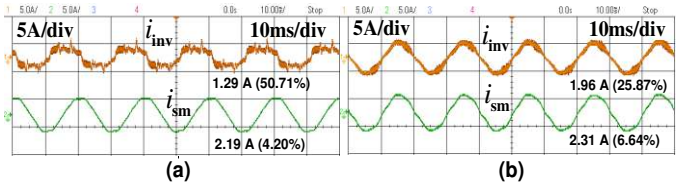

Fig. 26. i_{inv} and i_{sm} of VSI and SQIM with filter at 50 Hz in (a) PM, (b) SM when "n" is connected with "o".

F. Reduction of dv/dt at motor terminal

The effect of higher value of filter capacitance on *dv/dt* reduction in PM than SM has been shown through experimental results. The *dv/dt* without LC filter is around 20 kV/µs for V_{dc} of 600 V and 30 ns fall time as shown in Fig. 27 (c). The maximum time derivative of the stator line-line voltage in SM and PM as shown in Fig. 27 (a) and (b) are around 16 V/µs and 2.8 V/µs, respectively. It is well below the permissible *dv/dt* limit as specified by IEC 60034 or NEMA MG1 standard for motor voltage (≤ 600 V). Therefore, the proposed sinusoidal filter is not only filtering out the resonance frequency components of the output voltage of VSI by but also reducing the *dv/dt* at the motor-input terminals. This additional *dv/dt* reduction by the sinusoidal filter designed by PM is very useful in SiC MOSFET based VSI switching at very high frequency.

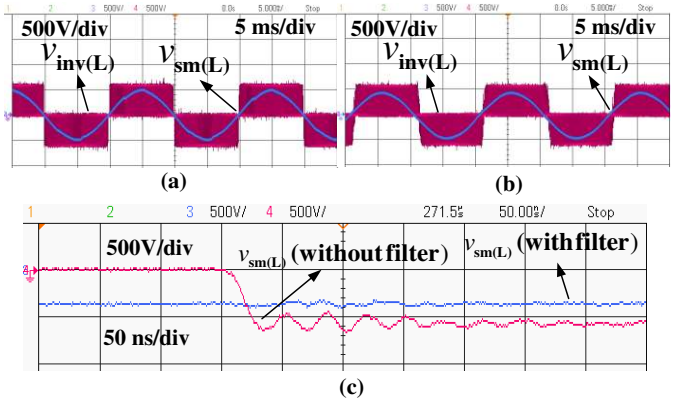

Fig. 27. Line-line voltage of VSI and SQIM with filter in (a) SM and (b) PM, (c) Line-line voltage of SQIM without and with filter designed by PM.

V. STABILITY OF CLOSED-LOOP DRIVE WITH FILTER

If the bandwidth of the inner *d*- and *q*-axis stator-current loop of a rotor-flux oriented control (RFOC) of SQIM drive with LC filter is close to the effective resonance frequency of the LCL network, it may happen that the closed-loop system becomes unstable at certain operating points due to the resonant frequency oscillations. These oscillations are generally damped out by different active damping (AD) techniques [22] and [34]. A simple inverter-current based AD technique is proposed in [34] where the virtual series resistances connected with the filter inductors are emulated in control and thus the unstable operating points have been stabilized by damping out the resonance frequency oscillations. The high-frequency components of the inverter-current are extracted by high-pass filters and multiplied by damping gain (K_{damp}) to construct the *d*- and *q*-axis compensating terms. These terms are then subtracted from the output voltage references of the *d*- and *q*-axis stator-current PI controllers. In this AD control, there is no need to change the parameters of the PI controllers of RFOC of SQIM without the filter. The value of K_{damp} has to be chosen wisely to ensure the stability of the drive at all operating points. The AD technique is not discussed here in detail as it has been thoroughly explained in [34]. Therefore, it has been directly used in this paper to analyze the stability of the drive at a certain operating point.

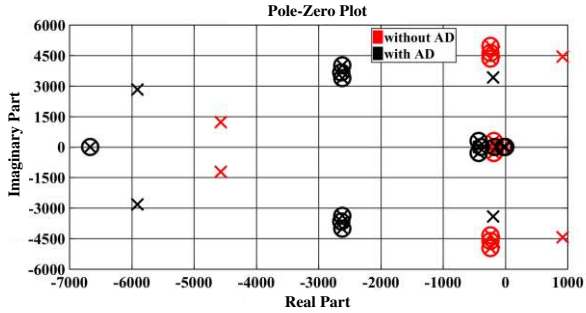

Fig. 28. Poles and zeros of *d*-axis CLTFs without and with AD.

The poles (×) and zeros (o) of *d*- and *q*-axis of inner stator-current closed-loop transfer functions (CLTFs) in RFOC of

SQIM and filter (PM) without and with AD at ω_e = 300 rad/s have been plotted in the complex *s*-plane as shown in Figs. 28 and 29. It is observed from the pole-zero plots of the *d*- and *q*-axis CLTFs without AD that there are two right half poles and the operating point is unstable. However, those right half poles have been shifted to the left half *s*-plane after applying AD and the unstable operating point is stabilized. The value of K_{damp} is chosen as 8 and the bandwidth of the inner current loop is 750 Hz which is closer to the effective resonant frequency.

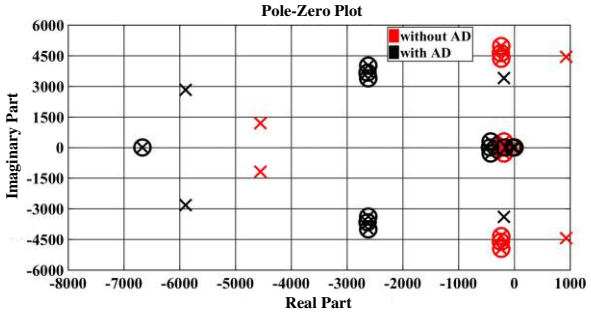

Fig. 29. Poles and zeros of *q*-axis CLTFs without and with AD.

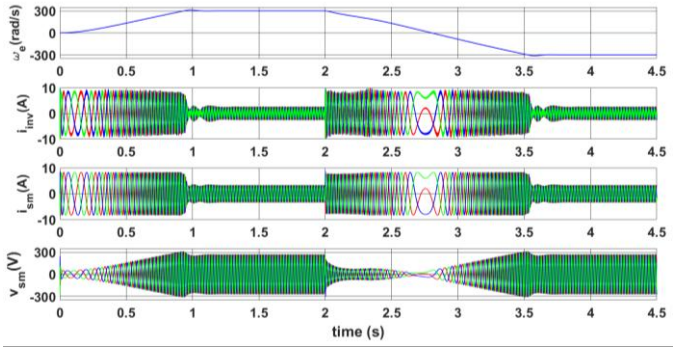

Fig. 30. Waveforms of ω_e, i_{inv}, i_{sm}, and v_{sm} of SQIM during start-up and speed-reversal in RFOC of the drive (SQIM + Filter) in PM with AD.

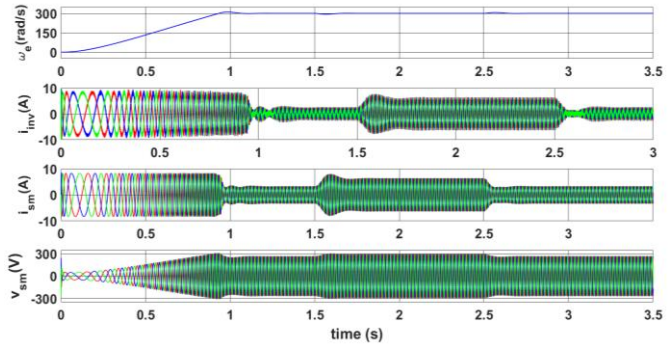

Fig. 31. Waveforms of ω_e, i_{inv}, i_{sm}, and v_{sm} of SQIM in RFOC of the drive (SQIM + Filter) in PM with AD when the load is applied at 1.5 s and removed at 2.5 s.

RFOC of the drive (SQIM +filter (PM)) with AD technique [34] has been simulated in MATLAB Simulink to check its steady-state and dynamic performance and corresponding simulation results (inverter-current (i_{inv}), stator-current (i_{sm}), electrical speed (ω_e), and stator-phase-voltage (v_{sm}) of SQIM) for two cases are presented. In Fig. 30, the motor is started from the zero speed with electrical-speed reference of 300 rad/s at no-load and it reaches the desired speed. Thereafter, the speed reference has been changed at 2 s from 300 rad/s to −300 rad/s. In Fig. 31, the motor is started with a speed reference of 300 rad/s at no-load. Thereafter, a sudden load is applied at 1.5 s and then removed at 2.5 s. In both cases, all the resonance frequency components have been damped out by the AD technique and the drive gives satisfactory performance during start-up, speed-reversal, no-load, and full load operation.

The instantaneous active power of the inverter and SQIM (P_{inv} and P_{sm}), and the instantaneous reactive power of the inverter and SQIM (Q_{inv} and Q_{sm}) have been calculated from the α and β components of the voltage references and currents of the inverter, and the stator-voltages and stator-currents of the SQIM as given by

$$P_{inv} = \frac{2}{3}\left(v_{inv\alpha} i_{inv\alpha} + v_{inv\beta} i_{inv\beta}\right) \tag{18}$$

$$Q_{inv} = \frac{2}{3}\left(v_{inv\beta} i_{inv\alpha} - v_{inv\alpha} i_{inv\beta}\right) \tag{19}$$

$$P_{sm} = \frac{2}{3}\left(v_{s\alpha} i_{s\alpha} + v_{s\beta} i_{s\beta}\right) \tag{20}$$

$$Q_{sm} = \frac{2}{3}\left(v_{s\beta} i_{s\alpha} - v_{s\alpha} i_{s\beta}\right) \tag{21}$$

The average reactive power of the inverter (Q_{inv}) in Fig. 32 is almost zero at steady-state. However, the reactive power of the motor (Q_{sm}) in Fig. 32 is not zero at steady-state as expected. Moreover, the active power of the inverter (P_{inv}) and the active power of the motor (P_{sm}) in Fig. 32 follow each other as expected. It shows that the filter capacitor in PM is able to supply the steady-state reactive power demand of the SQIM at 300 rad/s at no-load and full load operation without drawing reactive power from inverter ac-side.

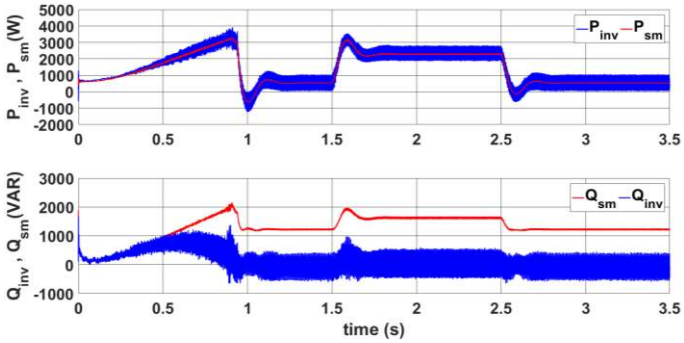

Fig. 32. Active power (P_{inv}), reactive power (Q_{inv}) of Inverter and active power (P_{sm}), reactive power (Q_{sm}) of SQIM in RFOC of the drive (SQIM + Filter) in PM with AD when the load is applied at 1.5 s and removed at 2.5 s.

VI. Conclusions

A new methodology of designing sinusoidal LC filter is proposed for the PWM VSI fed SQIM drive where the reactive power demand of the motor is supplied from the filter capacitor in addition to its high-frequency filtering capability. The increased size of the filter capacitor in PM than SM is compensated by the advantageous impacts of the filter on the drive. The impacts of the LC filters designed by SM and PM on the SQIM drive have been discussed, analyzed, and verified experimentally with in-house designed and developed SiC MOSFET based VSI fed SQIM drive. The filter, designed by PM, reduces the switch current of the VSI, the total power loss

in the drive, the distortions in the stator flux trajectory, *dv/dt* at motor terminals, and the air-gap torque pulsation of the SQIM as compared to SM. The high-frequency ripple current components in the dc-link capacitor current are also reduced in PM as compared to SM resulting in lesser ESR loss and lesser temperature rise of the dc-link capacitor. The common mode voltage can also be reduced in PM than SM when the neutral point of the filter capacitors is connected with the mid-point of the dc-link at the cost of increased ripple in dc-link and inverter current. The unstable operating point of RFOC of SQIM drive with LC filter has been stabilized by AD technique and simulation results have been presented to verify the steady-state and dynamic performances of the drive. Although the paper discusses the proposed method with SiC MOSFET based VSI, it may also be used with Si MOSFET based VSI.

REFERENCES

[1] J. Millán, P. Godignon, X. Perpiñà, A. Pérez-Tomás, and J. Rebollo, "A survey of wide bandgap power semiconductor devices", *IEEE Trans. Power Electron.*, vol. 29, no. 5, pp. 2155–2163, May 2014.

[2] B. J. Biela, M. Schweizer, S. Waffler, and J.W Kolar, "SiC versus Si—Evaluation of potentials for performance improvement of inverter and DC–DC converter systems by SiC power semiconductors", *IEEE Trans. Ind. Electron.*, vol.58, no.7, pp. 2872–2882, July 2011.

[3] J. Rabkowski, D. Peftitsis, and H. Nee, "Silicon carbide power transistors: A new era in power electronics is initiated," *IEEE Ind. Electron. Mag*., vol. 6, no. 2, pp. 17–26, June 2012.

[4] A. Bindra, "Wide-Bandgap-Based Power Devices: Reshaping the power electronics landscape", *IEEE Power Electron. Mag*., vol. 2, no. 1, pp. 42–47, March 2015.

[5] N. C. Sintamarean, F. Blaabjerg, H. Wang, Y. Yang, "Real field mission profile oriented design of a SiC-based PV-inverter application", *IEEE Trans. Ind. Appl.*, vol. 50, no. 6, pp. 4082–4089, Nov./Dec. 2014.

[6] D. Gerada, A. Mebarki, N. L. Brown, C. Gerada, A. Cavagnino, and A. Boglietti, "High-Speed Electrical Machines: Technologies Trends and Developments", *IEEE Trans. Ind. Electron.*, vol. 61, no. 6, pp. 2946–2959, June 2014.

[7] K. Hamada, M. Nagao, M. Ajioka, and F. Kawai, "SiC-Emerging Power Device Technology for Next-Generation Electrically Powered Environmentally Friendly Vehicles," *IEEE Trans. Electron Devices*, vol. 62, no. 2, pp. 278–285, Feb. 2015.

[8] E. Person, "Transients Effects in Application of PWM Inverters to Induction Motors", *IEEE Trans. Ind. Appl.*, vol. 28, no. 5, pp.1095–1101, May 1992.

[9] A.H. Bonnett, "Analysis of the Impact of Pulse-Width Modulated Inverter Voltage Waveforms on AC Induction Motors", *IEEE Trans. Ind. Appl.*, vol. 32, no. 2, pp. 386–392, March/April 1996.

[10] S. Chen, T. A. Lipo, and D. Fitzgerald, "Source of induction motor bearing currents caused by PWM inverters", *IEEE Trans. Energy Conversion*, vol. 11, no. 1, pp. 25–32, Mar. 1996.

[11] G. Skibinski, R. Kerkman, D. Schlegel, "EMI emissions of modern PWM ac drives", *IEEE Ind. Appl. Mag*., vol. 5, no. 6, pp. 47–80, Nov./Dec. 1999.

[12] H. W. van der Broeck, H.-Ch. Skudelny, "Analytical analysis of the harmonic effects of a PWM ac drive", *IEEE Trans. Power Electron*., vol. 3, no. 2, pp. 216–223, 1988.

[13] C. Choochuan, "A survey of output filter topologies to minimize the impact of PWM inverter waveforms on three-phase ac induction motors," in *Proc. 7th Int. Power Eng. Conf. (IPEC'05)*, pp. 1–6, Nov. 29/Dec. 2, 2005.

[14] N. Hanigovszki, J. Landkildehus, F. Blaabjerg, "Output filters for ac adjustable speed drives", *Proc. IEEE APEC*, pp. 236–242, 2007.

[15] J. K. Steike, "Use of an LC filter to achieve a motor-friendly performance of the PWM voltage source inverter", *IEEE Trans. Energy Convers.*, vol. 14, no. 3, pp. 649–654, Sep. 1999.

[16] H. Akagi, H. Hasegawa, and T. Doumoto, "Design and performance of a passive EMI filter for use with a voltage source PWM inverter having sinusoidal output voltage and zero common-mode voltage", *IEEE Trans. Power Electron*., vol. 19, no. 4, pp. 1069–1076, Jul. 2004.

[17] S. Pöhler, A. Mertens, and R. Sommer, "Optimisation of Output Filters for Inverter Fed Drives" *Proc. IEEE-IECON Conf.*, pp. 1082–1088, Nov. 2006.

[18] Mario Cacciato, Giuseppe Scarcella, Giacomo Scelba, Gaetano Pecoraro,"Genetic algorithms based design technique of sine wave filters for AC motor drives", *IEEE ELEKTRO*, pp. 208–213, 19–20 May 2014.

[19] C. Xivou. Y.Binl, and G. Yu. "The engineering design and optimization of inverter output RLC filter in AC motor drive system", *Proc. IEEE IECON Conf.*, pp. 175–180, 2002.

[20] T. C. Y. Wang, Z. Ye, G. Sinha, and X. Yuan, "Output filter design for a grid interconnected three-phase inverter," in *Proc. IEEE Power Electron. Spec. Conf.*, vol. 2, pp. 779–784, 2003.

[21] M. Swamy, J. Kang, and K. Shirabe, "Power loss, system efficiency and leakage current comparison between Si IGBT VFD and SiC FET VFD with various filtering options", *IEEE Trans. Ind. Appl*., vol. 51, no. 5, pp. 3858–3866, Sep./Oct. 2015.

[22] K. Hatua, A. K. Jain, D. Banerjee, and V. T. Ranganathan, "Active damping of output LC filter resonance for vector-controlled VSI-fed AC motor drives", *IEEE Trans. Ind. Electron.*, vol. 59, no. 1, pp. 334–342, Jan. 2012.

[23] P. Mishra, R. Maheshwari, "LC filter Design Method for Pulse Width Modulated Inverter Fed Induction Motor Drive", *IEEE iTEC INDIA-2017*, 13−15 Dec. 2017.

[24] J. Huppunen, J. Pyrhonen, "Filtered PWM-inverter drive for high-speed solid-rotor induction motor", *Conf. Rec. IEEE IAS Annu. Meeting*, vol. 3, pp. 1942–1949, Oct. 2000.

[25] Jing Guo, "Modeling and design of inverters using novel power loss calculation and dc-link current/voltage ripple estimation methods and bus bar analysis", Ph.D. dissertation, Mcmaster University, 2017.

[26] J. W. Kolar, S. D. Round, "Analytical calculation of the RMS current stress on the DC-link capacitor of voltage-PWM converter systems", *Proc. Inst. Electr. Eng. Electr. Power Appl.*, vol. 153, no. 4, pp. 535–543, Jul. 2006.

[27] Datasheet (Part No: BLC160J901B4C), [Online]. Available: http://www.cde.com/resources/catalogs/BLC.pdf.

[28] H. Wang, F. Blaabjerg , "Reliability of capacitors for DC-link applications in power electronic converters—An overview", *IEEE Trans. Ind. Appl*., vol. 50, no. 5, pp. 3569-3578, Sep./Oct. 2014.

[29] N.R.N, Idris, and A.H.M. Yatim, "An improved stator flux estimation in steady-State operation for direct torque control of induction machines", *IEEE Trans. Ind. Appl*., vol. 38, No. 1, pp. 110–116, 2002.

[30] J. Song-Manguelle et al., "Analytical expression of pulsating torque harmonics due to PWM drives", *Proc. ECCE*, pp. 2813–2820, Sep. 2013.

[31] D. A. Rendusara and P. N. Enjeti, "An improved inverter output filter configuration reduces common and differential modes dv/dt at the motor terminals in PWM drive systems", *IEEE Trans. Power Electron*., vol. 13, no. 6, pp. 1135–1143, Nov. 1998.

[32] T. G. Habetler, R. Naik, and T. A. Nondahl, "Design and implementation of an inverter output LC filter for dv/dt reduction", *IEEE Trans. Power Electron.*, vol. 17, pp. 327–331, May 2002.

[33] Y. Murai, T. Watanabe, and H. Iwasaki, "Waveform distortion and correction circuit for PWM inverters with switching lag-times", *IEEE Trans. Industry Applications*, pp. 881–886, 1987.

[34] P. Mishra, R. Maheshwari, and D. Patil, "Stabilization of Rotor Flux Oriented Control of Induction Motor with Filter by Active Damping", *IEEE Trans. Ind. Electron.*, 20 Dec. 2018 (Early Access).

Prasun Mishra (M'19) was born in West Bengal, India. He received the B.Tech. degree in electrical engineering from Haldia Institute of Technology, West Bengal, India in 2010 and the M.Tech. degree in mechatronics from the Academy of Scientific and Innovative Research, New Delhi, India in 2013. From 2010 to 2011, he was with Tata Consultancy Services, Bangalore, India. From 2011 to 2014, he was Scientist Trainee at CSIR Central Mechanical Engineering Research Institute, West Bengal, India, with Quick Hire Scientist (trainee) fellowship. He is currently working toward the Ph.D. degree at Power Electronics, Electrical Machines and Drives Group, Department of Electrical Engineering, Indian Institute of Technology Delhi, New Delhi, India. His research interests include

design of power electronics converter, modelling and control of electric drives.

Ramkrishan Maheshwari (S'10–M'11–SM18) was born in Allahabad, India. He received the master of engineering (M.E.) degree in electrical engineering from the Indian Institute of Science (IISc), Bangalore, India in 2005 and the Ph.D. degree in electrical engineering from Aalborg University, Aalborg, Denmark in 2012. From 2005 to 2008, he was with Honeywell Technology Solution Lab, Bangalore, India. From 2012 to 2014, he was with the Department of Energy Technology, Aalborg University, Denmark. He is currently working as an assistant professor with the Department of Electrical Engineering, Indian Institute of Technology, New Delhi, India. His research interests include modeling and control of power converters.